REPORT DOCUMENTATION PAGE

Form Approved OMB NO. 0704-0188

1. REPORT DATE (DD-MM-YYYY)	2. REPORT TYPE	3. DATES COVERED (From - To)
	New Reprint	-

4. TITLE AND SUBTITLE

Analysis of Double Layer and Adsorption Effects at the Alkaline Polymer Electrolyte-Electrode Interface

5a. CONTRACT NUMBER

W911NF-09-1-0227

5b. GRANT NUMBER

5c. PROGRAM ELEMENT NUMBER

611102

6. AUTHORS

Murat Ünlü, Daniel Abbott, Nagappan Ramaswamy, Xiaoming Ren, Sanjeev Mukerjee, Paul A. Kohl

5d. PROJECT NUMBER

5e. TASK NUMBER

5f. WORK UNIT NUMBER

7. PERFORMING ORGANIZATION NAMES AND ADDRESSES

Northeastern University
Office of Sponsored Programs
360 Huntington Ave., 405 Lake Hall
Boston, MA 02115 -5000

8. PERFORMING ORGANIZATION REPORT NUMBER

9. SPONSORING/MONITORING AGENCY NAME(S) AND ADDRESS(ES)

U.S. Army Research Office
P.O. Box 12211
Research Triangle Park, NC 27709-2211

10. SPONSOR/MONITOR'S ACRONYM(S)

ARO

11. SPONSOR/MONITOR'S REPORT NUMBER(S)

55036-CH.7

12. DISTRIBUTION AVAILIBILITY STATEMENT

Approved for public release; distribution is unlimited.

13. SUPPLEMENTARY NOTES

The views, opinions and/or findings contained in this report are those of the author(s) and should not contrued as an official Department of the Army position, policy or decision, unless so designated by other documentation.

14. ABSTRACT

In this study, the performance of the anionic electrodes in polymer-based alkaline fuel cells is analyzed. Direct alcohol, alkaline fuel cells suffer from a rapid decrease in cell potential at low discharge currents. Several effects are described to account for this drop in cell potential. Quaternary ammonium ions can specifically adsorb on the catalyst surface decreasing the active surface area and lowering the rate of methanol oxidation. In addition, the tethering of the quaternary ammonium cations on the polymer electrolyte inhibits the cation mobility causing a

15. SUBJECT TERMS

Anion Exchange Membrane, Alkaline Fuel Cell, Ammonium ion poisoning

16. SECURITY CLASSIFICATION OF:			17. LIMITATION OF ABSTRACT	15. NUMBER OF PAGES	19a. NAME OF RESPONSIBLE PERSON
a. REPORT	b. ABSTRACT	c. THIS PAGE			Sanjeev Mukerjee
UU	UU	UU	UU		19b. TELEPHONE NUMBER 617-373-2382

Report Title

Analysis of Double Layer and Adsorption Effects at the Alkaline Polymer Electrolyte-Electrode Interface

ABSTRACT

In this study, the performance of the anionic electrodes in polymer-based alkaline fuel cells is analyzed. Direct alcohol, alkaline fuel cells suffer from a rapid decrease in cell potential at low discharge currents. Several effects are described to account for this drop in cell potential. Quaternary ammonium ions can specifically adsorb on the catalyst surface decreasing the active surface area and lowering the rate of methanol oxidation. In addition, the tethering of the quaternary ammonium cations on the polymer electrolyte inhibits the cation mobility causing a diffuse double layer to be formed. The diffuse double layer electrostatically inhibits the migration of hydroxide to the surface of the electrode which is needed for alcohol oxidation.

REPORT DOCUMENTATION PAGE (SF298)
(Continuation Sheet)

Continuation for Block 13

ARO Report Number 55036.7-CH
Analysis of Double Layer and Adsorption Effects ...

Block 13: Supplementary Note

Approved for public release; distribution is unlimited.

Journal of The Electrochemical Society, **158** (11) B1423-B1431 (2011)
0013-4651/2011/158(11)/B1423/9/$28.00 © The Electrochemical Society

Analysis of Double Layer and Adsorption Effects at the Alkaline Polymer Electrolyte-Electrode Interface

Murat Ünlü,[a,*] Daniel Abbott,[b] Nagappan Ramaswamy,[b,*] Xiaoming Ren,[c] Sanjeev Mukerjee,[b] and Paul A. Kohl[a,,z]**

[a]*School of Chemical and Biomolecular Engineering, Georgia Institute of Technology, Atlanta, Georgia 30332-0100, USA*
[b]*Northeastern University, Department of Chemistry and Chemical Biology, Boston, Massachusetts 02115-5005, USA*
[c]*US Army Research Laboratory, Adelphi, Maryland 20783, USA*

In this study, the performance of the anionic electrodes in polymer-based alkaline fuel cells is analyzed. Direct alcohol, alkaline fuel cells suffer from a rapid decrease in cell potential at low discharge currents. Several effects are described to account for this drop in cell potential. Quaternary ammonium ions can specifically adsorb on the catalyst surface decreasing the active surface area and lowering the rate of methanol oxidation. In addition, the tethering of the quaternary ammonium cations on the polymer electrolyte inhibits the cation mobility causing a diffuse double layer to be formed. The diffuse double layer electrostatically inhibits the migration of hydroxide to the surface of the electrode which is needed for alcohol oxidation.
 [DOI: 10.1149/2.075111jes]

Manuscript submitted June 15, 2011; revised manuscript received July 28, 2011. Published October 5, 2011.

Alkaline fuel cells using polymer-based anion exchange membranes (AEM) are an attractive alternative to proton exchange membrane (PEM) fuel cells.[1,2] From electrocatalysts standpoint, alkaline environment primarily serves to stabilize some non-noble metal surfaces against corrosion as evidenced by the Pourbaix diagrams and furnishes the much required window of opportunity to utilize non-noble metals as electrode materials.[3] The widely claimed aspect of so-called facile kinetics in alkaline media remains quite unjustified since such comparisons have usually been made between phosphoric acid fuel cells (containing specifically adsorbing phosphate anions in addition to oxide formation) and liquid alkaline fuel cells.[4] Further, it was recently shown that on carbon supported polycrystalline platinum catalysts, both hydrogen oxidation reaction (HOR),[5] and oxygen reduction reaction (ORR)[6,7] suffer higher overpotential losses in alkaline media (0.1 M K/NaOH) compared to non-adsorbing acidic electrolytes (0.1 M $HClO_4$). In alkaline media, the slower HOR kinetics was attributed to the stronger Pt-H_{ads} bond strength,[8] whereas the slower ORR kinetics was attributed to higher coverage of specifically adsorbed hydroxide anions compared to acidic media.[7] With regards to electrocatalysis of ORR on non-Pt catalysts, the only advantage in alkaline media is the improved stabilization of the peroxide anion (HO_2) reaction intermediate compared to acidic conditions (H_2O_2) which leads to lower ORR overpotentials on non-Pt catalysts in alkaline media.[7,9,10] In contrast to HOR kinetics, the methanol oxidation reaction (MOR) kinetics on Pt and PtRu based catalysts has been shown to be higher in alkaline media (0.1 M NaOH) by a factor of ∼10–15 based on mass-specific current density values compared to acidic media (0.5 M H_2SO_4).[11] However, compared to a non-adsorbing acidic electrolyte (0.1 M $HClO_4$) the activation energy for MOR in alkaline media (0.1 M KOH) was found to be ∼10–15 times greater than that in acidic media.[12] The higher pH does allow a greater number of metals to be considered, as evidenced by the use of non-platinum based electrodes, such as nickel-based anodes[13] and silver-based cathodes.[14,15]

From alkaline membrane standpoint, several potential advantages such as lower degree of fuel crossover in-part due to the opposite direction of electro-osmotic drag in an AEM cell compared to a PEM cell, and subdued peroxide radical initiated membrane degradation.[16] Absence of alkali metal ions in AEM's also prevent the precipitation of insoluble carbonate salts in the porous electrode structure, although the ion exchange of carbonate anions in the AEM and the accompanying loss in ion mobility cannot be prevented. Additionally, novel AEM/PEM hybrid designs simplify the water management and enable fuel cell operation without external humidification.[17]

State of the art PEM fuel cell performance operating on H_2/air gas feeds using Pt-based catalysts yield power densities of ∼700 mW/cm^2 at 0.65 V (80°C, 100% RH).[18] In comparison, analogous AEM fuel operating on H_2/CO_2-free air gas feeds yields power densities of ∼275 mW/cm^2 at 0.65 V (50°C, 85% RH).[19] While the power densities achieved in the current state of the art H_2-fed AEM fuel cells is less than half that in PEM fuel cells, it is indeed promising considering the fact that i) the mobility of hydroxide anions is lower than that of protons, and (ii) the alkaline ionomer solutions used in the catalyst layer are only in their nascent stage of development.

Despite all the above considerations, a more chronic problem in the development of alkaline fuel cells has been the very poor performance of direct alcohol (KOH-free anode feed) AEM fuel cells.[20] In particular, alkali metal free, direct methanol AEM fuel cells have shown power densities less than 8 mW cm^{-2}, in spite of the generous use of platinum in the electrode structures.[21–24] Varcoe and Slade reported a power density of 8 mW cm^{-2} for methanol using 2.5 bar back-pressure at 80°C.[25] They note that the addition of alkali metal hydroxide to the methanol improved the performances when CO_2 free oxygen was used at the cathode. Bunazawa and Yamazaki have tested an AEM cell with PtRu at the anode and Pt at the cathode with 1 M MeOH at 80°C. The peak power density was 7.6 mW cm^{-2}, however, it increased to 59 mW/cm^2 when 0.5 M NaOH was added to the fuel.[21] In the report by Coutanceau et al., the peak power density for 1 M methanol was 0.2 mW cm^{-2} and the power density improved to 18 mW cm^{-2} with 4 M NaOH in the fuel.[22] In addition to methanol, several other fuels with metal hydroxide addition have been used in AEM fuel cells. Li et al. recently reported 60 mW cm^{-2} for 3 M EtOH in 5 M KOH at 60°C using non-Pt catalysts.[26] Ethylene glycol fueled AEM fuel cell produced 28 mW cm^{-2} at room temperature.[27] The tests for ethylene glycol, glycerol, methanol, erythritol, and xylitol as fuel in 1 M KOH resulted in the power densities of 9.5, 6.5, 6.0, 5.5, and 4 mW cm^{-2}, respectively, at 50°C.[14,28]

We note that in each case, the performance is low in the absence of alkali metal hydroxide in the anode feed and dramatically improved with the addition of alkali metal hydroxide to the fuel. The addition of alkali metal ions to the fuel is not acceptable in a practical fuel cell system because CO_2 from the air and from the oxidation of methanol leads to the formation and precipitation of insoluble carbonates that catastrophically decrease performance. In addition, the added chemical components to the fuel decrease the system energy density. The need to dispose of the reaction products also increases the complexity of the fuel cell system and operation.

* Electrochemical Society Student Member.
** Electrochemical Society Fellow.
z E-mail: kohl@gatech.edu

In the absence of excess KOH in the anode feed, efficient fuel oxidation is dependent on the establishment of three-phase boundary at the active site between ionomer, carbon support, and reactant. The presence of excess KOH in the anode feed discredits the use of ionomer solutions in the catalyst layer by establishing the so-called "flooded electrolyte" system. There are several factors that can limit the AEM cell performance in the absence of excess KOH including low open circuit voltage, poor catalyst utilization, fuel (e.g. methanol) cross-over from the anode to the cathode, lower interfacial and bulk ionic conductivity of the ionomer membrane, and mass transfer resistance of the fuel to the anode catalyst. Several investigations using full-cell or half-cell tests have been conducted by modifying the ionomer content, type of catalyst, and additives in the electrode structure. However, these studies have not resulted in any conclusive results for explaining low power density in absence of alkali metal hydroxide.[21,23,29,30] MeOH oxidation studies were performed in half-cell systems varying the methanol and electrolyte concentrations.[31,32] In general, it was concluded that the addition of alkali metal ions to the electrolyte improves the rate of alcohol oxidation due to the higher pH, indicating that the pH in AEM matrix without the added alkali electrolyte may not be high enough. In addition, it has been proposed that there is an optimum ratio of OH to MeOH, which balances the removal of reaction intermediates and surface coverage of methanol and hydroxide.[33] However, a more fundamental understanding of the origin of the limited cell performances in AEM fuel cells remains elusive. Therefore, the primary objective of this research article is to unravel the various aspects that influence the charge transfer processes at the anode-alkaline membrane interface.

Experimental Methods

Membrane electrode assemblies (MEAs) were prepared using commercial PtRu (Alfa Aesar, 4.0 mg_{PtRu}/cm^2) or Pt (Alfa Aesar, 2.0 mg_{Pt}/cm^2) anodes on Toray paper, Pt/C cathode on Gas Diffusion Layer (GDL), Tokuyama AS4 ionomer solution, and Tokuyama A201 ionomer membrane. Commercial PtRu anodes were spray coated with an interfacial layer of 1.0 mg_{AS4}/cm^2 of alkaline ionomer on the top surface prior to hot pressing. To prepare the cathode, a catalyst ink composed of BASF 30% Pt/C dispersed in a water-alcohol mixture along with the requisite amount of ionomer (Tokuyama AS4) was sprayed on gas diffusion layer (GDL, ETEK-BASF). Typical cathode loading consisted of 1.0 mg_{Pt}/cm^2 with an ionomer content of 28.5% by weight of the catalyst. After drying the cathodes, a layer of interfacial ionomer was sprayed to achieve a loading of 1.0 mg_{AS4}/cm^2. Hot pressing of the electrodes together with a Tokuyama A-201 membrane was carried out at 60°C and 100 psig pressure for duration of four minutes. MEAs were then assembled in a fuel cell consisting of 5 cm^2 serpentine flow fields. Humidification of the MEA was performed for 2 hours by flowing N_2 (100% RH) at a cell temperature of 50°C. Higher duration of humidification was not preferred to avoid thermal degradation of the membrane and the ionomer layer. The operating temperature of the cell was typically set at 50°C and the cell was activated with H_2/O_2 (inlet temperatures of 55°C, 100% RH, 28 psig back pressure).

The hydrogen adsorption/desorption and methanol oxidation experiments on planar Pt disk electrodes were conducted using a traditional three-electrode cell at ambient temperature. The Pt disk electrode had a geometric surface area of 0.385 cm^2. The Pt electrode surface was polished with a 0.05 μm alumina slurry and sonicated in distilled water for 10 minutes. The electrode was then soaked in concentrated nitric acid and rinsed thoroughly. Ag/AgCl was the reference electrode and carbon cloth was used as the counter electrode. Tetramethylammonium hydroxide (TMAOH), sodium hydroxide (NaOH), and poly(diallyldimethylammonium hydroxide) (PTMAOH) were used as electrolytes. PTMAOH was prepared from poly(diallyldimethylammonium chloride) using an ion exchange column. The electrolyte solutions were stored under nitrogen to prevent contamination from atmospheric carbon dioxide. The flow of nitrogen over the solution was maintained throughout the experiments. The solutions were purged with nitrogen for 30 minutes before the electrode was immersed into solution. The electrode surface was equilibrated by sweeping the potential at a scan rate of 100 mV/s until steady-state behavior was obtained, ca. 25 cycles. Electrochemical measurements were made using a PAR Potentiostat/Galvonostat Model 2273.

Ammonium contamination studies were conducted on Pt/C modified glassy carbon electrodes. A catalyst ink was prepared from 25 mg of 30% Pt/C (BASF) in 10 mL Millipore H_2O and 10 mL isopropyl alcohol. Exactly 5 μL of ink was deposited on a glassy carbon rotating disk electrode (A_{geo} = 0.247 cm^2) to yield a total catalyst loading of 7.5 $\mu g_{Pt}/cm^2$. Prior to ink deposition, the electrode was polished with 0.05 μm alumina slurry and sonicated twice in a sonic bath for 30 seconds each in a 50:50 solution of Millipore H_2O and isopropyl alcohol. The reference electrode used was a reversible hydrogen electrode (RHE) prepared from a solution of 0.1 M KOH. At the beginning of each experiment, the electrode was cycled 20 times from 0.05 V to 1.2 V at 50 mV/s in 0.1 M KOH followed by five cycles at 20 mV/s. Absolute methanol was then added to the KOH solution to obtain a total MeOH concentration of 0.5 M. Methanol oxidation was then performed by holding the potential at 0.6 V vs. RHE for 900 seconds. Subsequently, an aliquot of a given contaminant was added to bring the total contaminant concentration to 1 mM and the potential was again held at 0.6 V for 900 seconds. This procedure was repeated for the remaining contaminant concentrations of 5, 10, 20, 40, 60, and 120 mM. A new ink coating was used in the study of each contaminant. Contaminants investigated included tetramethylammonium hydroxide (TMAOH, 25% w/w aq), tetraethylammonium hydroxide (TEAOH, 35% w/w aq), tetra-n-propylammonium hydroxide (TPAOH, 40% w/w aq.), and benzyltrimethylammonium hydroxide (BTMAOH, 25% w/w aq.) all from Alfa Aesar. Electrochemical measurements were made using an Autolab Potentiostat/Galvanostat Model PGSTAT30 (Metrohm USA).

The electrochemical behavior of the transition metal complexes were studied at an alkaline ionomer modified glassy carbon electrode. A glassy carbon rotating disk electrode (A_{geo} = 0.247 cm^2), after polishing and pretreatments described above, was allowed to dry after deposition of 5 μL of 5 wt.% anion exchange ionomer (Tokuyama AS4) on the surface. The electrode was placed in an argon saturated 0.1 M NaOH solution and subjected to 20 cycles from 0.05 V to 1.2 V at 50 mV/s and five cycles at 20 mV/s. 10 mM of $K_3Fe(CN)_6$ was then added to the solution and the solution was purged with argon for an additional 10 minutes before collecting data. This experiment was repeated using 10 mM $Co(NH_3)_6Cl_3$ in place of $K_3Fe(CN)_6$.

Results and Discussion

The focus of this study is on the low electrode performance in direct alcohol, AEM fuel cells, compared to Nafion®-based PEM cells. The addition of alkali metal hydroxide improves the cell performance,[12,13,24,25,27] but the results are less than optimal. It should be emphasized that the addition of excess KOH in the anode feed is highly undesirable given the alkali metal carbonate precipitation issues.[1]

The performance of a direct ethanol alkaline fuel cell was characterized with and without the presence of excess KOH in the anode fuel. Figure 1 shows the polarization and power density curves for an AEM fuel cell with an anode composed of 4.0 mg_{PtRu}/cm^2 + 1.0 mg_{AS4}, cathode composed of 30% Pt/C (1.0 mg_{Pt}/cm^2 + 28 wt.% AS4) + 1.0 mg_{AS4}, and Tokuyama A201 anion exchange membrane. The cell was first operated with 1 M EtOH anode feed, which was later changed to 1 M EtOH with 0.25 M KOH. The results shown in Figure 1 are typical of all prior reports wherein there is a low open circuit potential (OCP), severe drop in potential at low current density and low power density when operated in the absence of KOH. The OCP improved from 0.68 V to 0.85 V when KOH was added to the anode feed. In the absence of KOH the maximum power density was 1.7 mW cm^{-2} at 5 mA cm^{-2} and 0.335 V. The maximum power density improved to 22.4 mW cm^{-2} at 64 mA cm^{-2} and 0.350 V when KOH was added to the fuel. For comparison, Liang et al.[34] reported 23 mW cm^{-2} using 1 M EtOH with 1 M KOH anode feed and pure O_2 at 50°C with

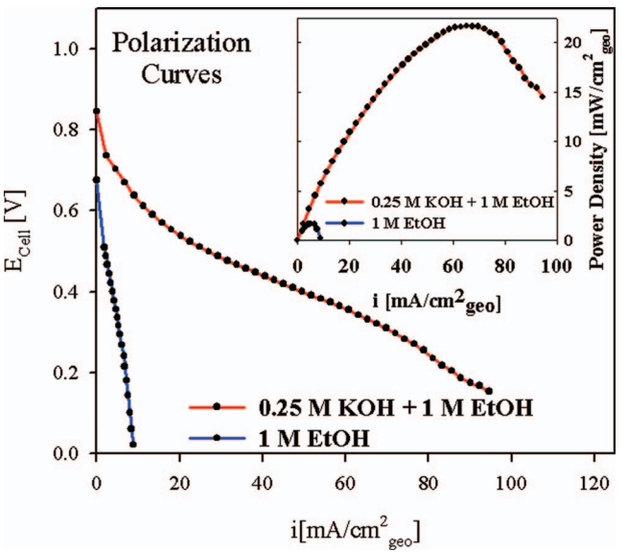

Figure 1. Direct ethanol fuel cell polarization curves taken at 50°C. Anode: PtRu on Toray paper (Loading = 4.0 mg_{Pt}/cm^2) with 1 mg_{AS4}/cm^2 interfacial ionomer film on surface. Cathode: 30% Pt/C on GDL (Loading = 1 mg_{Pt}/cm^2 + 28.5 wt% AS4 ionomer) with 1 mg_{AS4}/cm^2 interfacial film on surface. Tokuyama A-201 membrane. Anode feed: 1 M EtOH with/without 0.25 M KOH at 8 mL/min. Cathode feed: 100% RH O_2. Inset shows the corresponding power density curves.

a Tokuyama A201 membrane, 2.0 mg cm^{-2} HYPERMEC™ anode catalyst loading and 1.0 mg cm^{-2} HYPERMEC™ cathode catalyst loading. Fujiwara et al.[35] achieved a power density of 58 mW cm^{-2} using 3.0 mg_{PtRu} cm^{-2} with 5 wt.% anion exchange resin at the anode and a Tokuyama AEM when 1.0 M EtOH with 0.5 M KOH was used as the fuel. Only 8 mW cm^{-2} was obtained in the absence of KOH. Additionally, Hou et al.[36] reported power densities of ∼50 and ∼60 mW cm^{-2} at 75°C and 90°C, respectively, for a cell consisting of alkali metal hydroxide doped PBI membrane with 2.0 mg_{PtRu} cm^{-2} anode and 1.0 mg_{Pt} cm^{-2} loadings at the anode and cathode, respectively operating on 2 M EtOH in 2 M KOH anode feed. It should be noted that in each of the aforementioned studies,[34–36] a sharp drop in cell potential occurred at very low current densities followed by modest drop in cell potential as the current reached the mass transfer limited regime. In addition, the steep decline in potential at low cell current has also been observed in all fuel cells operating with methanol fuel supply[14,37–39] as well as studies with other alcohols.[14,37,38] These results indicate that the overall performance suffers significant cell voltage loss at low currents regardless of the choice of fuel. Moreover, the steep drop in potential has been observed for several different catalysts, including Pt/C,[37,40] Pt/Ti,[39] and PtRu.[14]

Figure 2 shows the AC impedance spectra of the fuel cell corresponding to Figure 1 taken with and without excess KOH in the anode feed. By plotting the imaginary versus real components of impedance, the charge transfer resistance, R_{CT}, was obtained after fitting the data to a semicircular curve and determining the difference between the high frequency and low frequency intercepts on the real axis. Similarly, the ionic resistance (R_{ionic}) of the membrane was determined from the x-intercept at the high frequency. It should be noted that the semicircular shape of the plot is indicative of the kinetically controlled region, while the absence of Warburg impedance, for the given potential and frequency range, suggests that the process is not diffusion controlled. When the cell was operated in the absence of KOH, it was found that R_{CT} and R_{ionic} were 84.25 and 2.95 Ω cm^2, respectively. The values obtained for the cell operated in the presence of KOH was R_{CT} = 6.55 Ω cm^2, and R_{ionic} = 0.55 Ω cm^2, which indicates that the ethanol oxidation kinetics were dramatically improved with the addition of KOH. A modest drop in R_{ionic} is expected in the presence of KOH since it increases the ionic conductivity of the membrane and the interface. The lower values for R_{CT} suggest that the rate of ethanol oxidation increased markedly with addition of KOH.

It is important to understand the source of performance loss in the absence of added KOH for each of the cell components. Typically, alkaline membrane fuel cells operating with H_2/O_2 achieve more than 500 mA cm^{-2} with similar cathode structures. Also, since the addition of KOH to the anode liquid fuel dramatically changes the AC impedance, it is reasonable to conclude that the performance of current alkaline alcohol fuel cells is primarily limited by anode performance. Further analysis of the alcohol oxidation anode was performed with an alcohol/H_2 half-cell system. Figure 3 shows the half-cell ethanol oxidation profile obtained from a cell operating with a 2.0 mg_{Pt}/cm^2 anode and the same cathode and membrane as described for the cell used in Figure 1. Humidified H_2 was used at the cathode which also served as the reference electrode. The maximum current density obtained for ethanol oxidation at 0.8 V was 5.7 mA cm^{-2} and 89.7 mA cm^{-2} in the absence and presence of 0.25 M KOH, respectively. Here, it can be seen that the rate of ethanol oxidation is significantly enhanced with

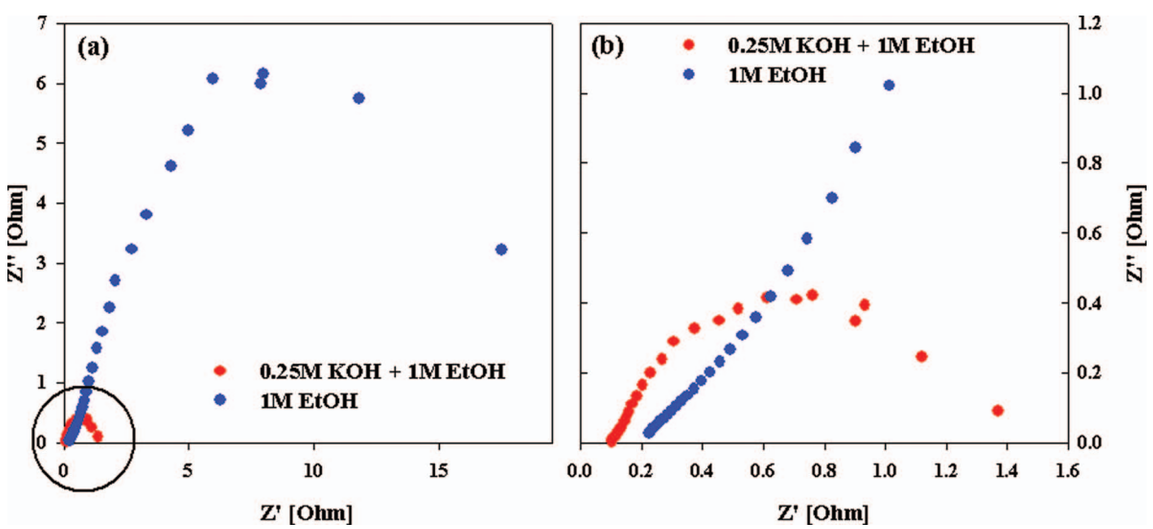

Figure 2. (a) Impedance spectra at 50°C collected at 0.4 V from 20 kHz to 0.1 mHz with an amplitude of 0.05 V. AEM fuel cell configuration same as that in Figure 1. Anode feed: 1 M EtOH with/without 0.25 M KOH at 8 mL/min. Cathode feed: 100% RH O_2. (b) Magnified plot of the circled region in (a).

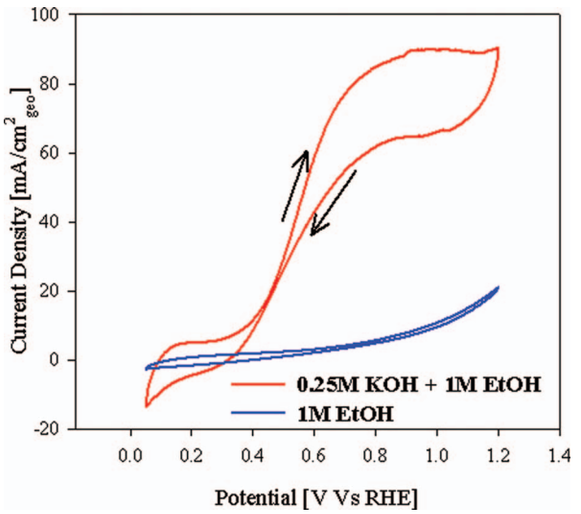

Figure 3. Ethanol oxidation curve at 50°C. Scan rate: 20 mV/s. Anode: Pt on Toray paper (Loading = 2.0 mg_{Pt}/cm^2) with 1mg_{AS4}/cm^2 ionomer film on surface. Cathode: 30% Pt/C on GDL (Loading = 1 mg_{Pt}/cm^2 + 28.5 wt.% AS4 ionomer) with 1mg_{AS4}/cm^2 ionomer film on surface. Tokuyama A-201 membrane. Anode feed: 1M EtOH with/without 0.25 M KOH at 8 mL/min. Cathode feed: O_2 100% RH.

excess KOH. No clear onset potential for ethanol oxidation could be discerned in Figure 3 in the absence of KOH from the anode feed. This half-cell result shows that the anodic oxidation of alcohol in the absence of excess KOH is a major limiting factor in the performance of alkaline direct alcohol fuel cells.

The half cell measurements and the impedance studies presented above show that the voltage drop at low current in the fuel cell is primarily isolated to the anode and not the cathode. The low performance in direct alcohol alkaline fuel cells could be attributed to several factors including lack of ionic conductivity in the anion exchange membrane, incomplete oxidation of small alcohol fuels, fuel crossover, and carbonate formation. Though each of these potential sources for the voltage drop at low current would have a negative effect on cell performance, it is unlikely that any of these could account for such a large difference in performance between alkaline direct alcohol fuel cells and their acidic counterparts. Thus, other factors should be considered in order to account for these performance losses in the absence of KOH.

In contrast to liquid alkaline electrolytes, an operating AEM fuel cell involves the use of interfacial alkaline ionomer solution in the catalyst layer to establish the three phase boundary required for electrocatalysis. This alkaline ionomer solution consists of immobile positive charges fixed to the polymer backbone and relatively mobile negative counter anions. Given that under conventional three-electrode configuration in liquid alkaline electrolytes alcohol oxidation takes place at appreciable rates, in this study we turn our attention to the anode double layer structure and anode catalyst/AEM ionomer interface. The Pt/electrolyte interface at a planar electrode in alkaline electrolytes was analyzed where mass transport limitations and variations in surface morphology are negligible. Additionally, the possible interaction of the components in the AEM ionomers with the Pt surface was evaluated separately. Figure 4 shows cyclic voltammograms on polycrystalline smooth Pt electrodes in 0.1 M NaOH and TMAOH electrolytes. The electrode surface was conditioned by cycling the potential until steady state performance was established. The initial scan direction was toward negative potentials starting at 0 V. The voltammograms were collected after two hours equilibration at the rest potential. The onset potential for hydrogen adsorption and desorption is essentially the same in the two electrolytes since they are both strong bases. The peak shape was similar for the two electrolytes, however, the total oxidative charge passed on the positive-going potential sweep after scan reversal at 1.05 V was greater for NaOH than for TMAOH. The anodic peak at ca. −1.0 V is due to surface hydrogen desorption. Typically, the total charge due to oxidation of adsorbed hydrogen corresponds to the active surface area of the electrode.[41] The anodic hydrogen desorption peak area for NaOH is 2.6 times greater than that for TMAOH. The difference between the two oxidation peaks is due to the nature of the cations since the concentration of hydroxide in both cases is identical. Previously, changes in the hydrogen adsorption/desorption behavior have been reported for different ions, depending on their specific adsorption characteristics. The decrease in the H UPD charge density in TMAOH is attributed to the specific adsorption of quaternary ammonium ions on the active platinum surface resulting in a decrease in active surface area.

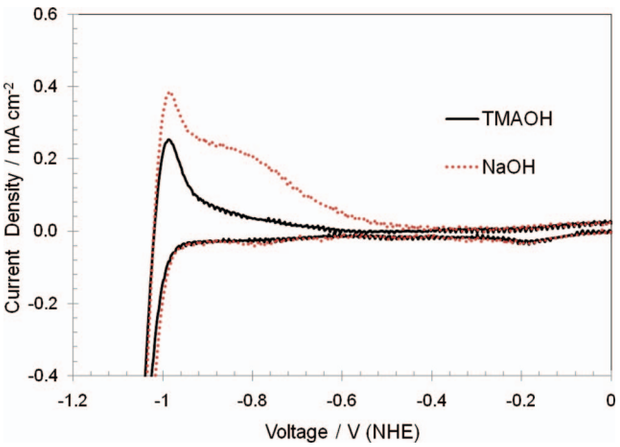

Figure 4. Cyclic voltammograms of smooth polycrystalline Pt electrodes in 0.1 M TMAOH or 0.1 M NaOH. The scan rate was 10 mV s^{-1}.

The adsorption of the tetramethylammonium cation onto the platinum surface was investigated as a function of time by examining the charge due to oxidative hydrogen desorption as a function of time, as shown in Figure 5. The peak area for hydrogen desorption decreased with the exposure time for the Pt electode in the solution. The peak area was calculated after 0.5, 1, 2, and 4 h in solution. The smaller oxidative peak is due to higher surface coverage of tetramethylammonium ions as a function of time. The peak area after 4 h was 4 times lower relative to the 30 min immersion. Quaternary ammonium cations have been categorized as weak adsorbates where the driving force is largely

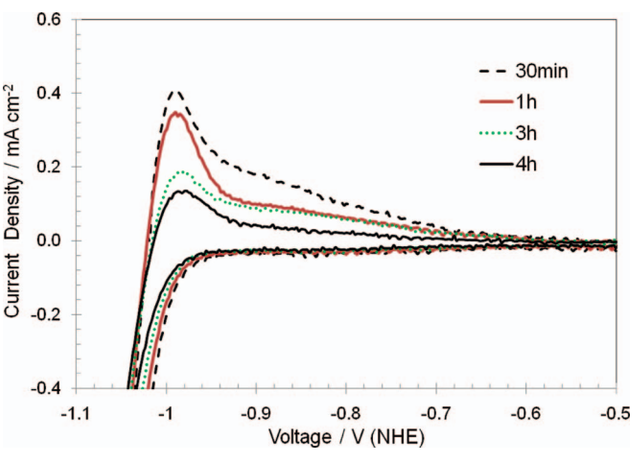

Figure 5. Cyclic voltammograms in 0.1 M TMAOH collected at various times after the electrode was immersed in the solution. The scan rate was 10 mV s^{-1}.

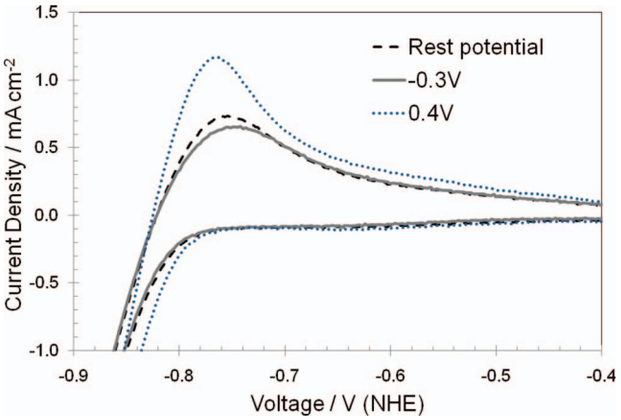

Figure 6. Cyclic voltammograms in 0.1 M TMAOH after the electrode potential was held at rest potential, −0.3, and 0.4 V for 20 min. Scan rate is 10 mV s^{-1}.

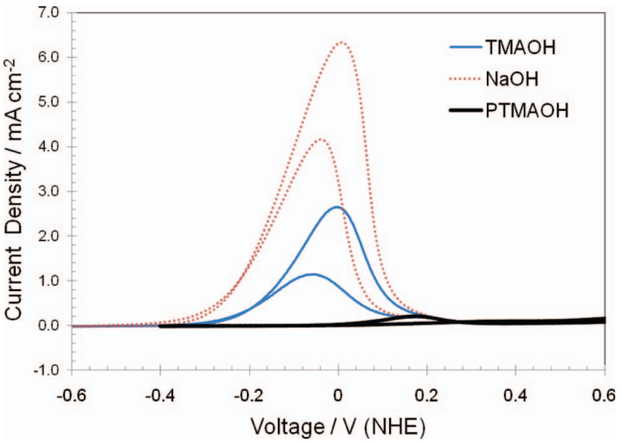

Figure 7. Cyclic voltammograms on Pt electrode for 1 M MeOH in 0.1 M TMAOH, NaOH and PTMAOH solutions. The scan rate is 10 mV s^{-1}.

due to electrostatic[42] interactions related to the solvation energy of the cations. Typically, the solvation energy for alkali and alkali earth cations is much higher than that for electrostatic adsorption. In contrast, quaternary ammonium ions are weakly solvated in water so that the electrostatic attraction with an oppositely charged surface favors adsorption. The specific adsorption of quaternary ammonium on Pt depends on the potential of zero charge (PZC) of platinum electrode in the reaction medium. There are two types of PZC, the potential of total charge (PZTC) and the potential of the zero free charge (PZFC). The latter one is believed to influence the double layer.[43,44] PZTC has been reported to be −0.110 V vs. NHE at pH 11.2,[45] −0.111 vs. NHE at pH 11.2,[46] and −0.4 V vs. NHE at pH 12.[47] PZFC has been estimated to be −0.39 at pH = 12 in the presence of KBr.[44] It is noteworthy that the PZC values depend on the adsorbate and specific adsorption of ammonium groups which are likely to shift PZFC to less (few decades of mV) negative values. These literature values show that the adsorbtion/desorption of hydrogen occurs at more negative potentials than PZTC and PZFC. This, electrostatically favors the adsorption of quaternary ammonium groups to the Pt surface. However, in addition to electrostatic interactions, it is also possible to have chemical interactions between methyl groups on the TMA^+ cation and the Pt surface.

The potential dependence of quaternary ammonium adsorption on the platinum electrode surface was evaluated by performing controlled-potential experiments. Preconditioning of the electrode at various potential was performed prior to the desorption experiment, as shown in Figure 6. First, the electrode was held at the open circuit potential (i.e. rest potential) and the oxidative hydrogen desorption voltammogram was recorded. When the electrode potential was preconditioned by holding it at 0.4 V vs. NHE for 20 min (a potential positive of PZC), the hydrogen oxidation peak increased in area. This increase in charge is due to a greater effective surface area from the electrostatic repulsion of the quaternary ammonium ions from the positively charged electrode surface. In contrast, the effective active surface area decreased when the electrode potential was held at −0.3 V vs. NHE for 20 min. When the electrode surface has negative excess charge, ammonium cations are attracted to the electrode surface, decreasing the available surface for hydrogen adsorption. This peak area dependence on the electrostatic interactions between the electrode and solvated ions plays an important role on the adsorption of TMA^+ ions on the platinum electrode.

The effect of the supporting electrolyte on methanol oxidation was evaluated on a planar platinum electrode. Figure 7 shows a series of voltammograms for methanol oxidation in NaOH and TMAOH two hours after immersion of Pt electrode into the solution. The current density for methanol oxidation in NaOH is substantially greater than in TMAOH. Moreover, the inhibition of methanol oxidation in TMAOH increases with time. Figure 8 shows the magnitude of the methanol oxidation peak as a function of time after immersion in solution. The peak current decreased with time and methanol oxidation was almost completely suppressed after 180 minutes after immersion in TMAOH. This observation is consistent with the decrease in hydrogen adsorption due to higher ammonium coverage with the time, shown in Figure 5. Moreover, when the electrode surface was mechanically polished after 220 min. immersion in TMAOH, the methanol oxidation reappeared. This result clearly shows that the surface coverage by ammonium species suppresses available catalytic area.

The experiments described above involved TMA^+ cations because benzyltrimethyl quaternary ammonium ions bound to a polymer backbone are the most chemical constituents of the current state of the art AEM ionomer solutions. It is of interest to evaluate alternative cations as the ion exchange sites on polymer backbones. The oxidation of methanol on platinum was studied as a function of the ammonium group adsorbed on the surface of the electrode. The first three cations studied were quaternary ammoniums with different length alkyl chains (methyl, ethyl and propyl). The fourth one was benzyltrimethyl ammonium hydroxide. The hydroxide salt of these quaternary ammonium cations was added to a 0.5 M MeOH solution. Then, the percent loss in current density after 900 sec potential control at 600 mV (vs. RHE) in 0.1 M KOH was recorded as a function of quaternary ammonium as shown in Figure 9. In general, all ammonium cations showed a

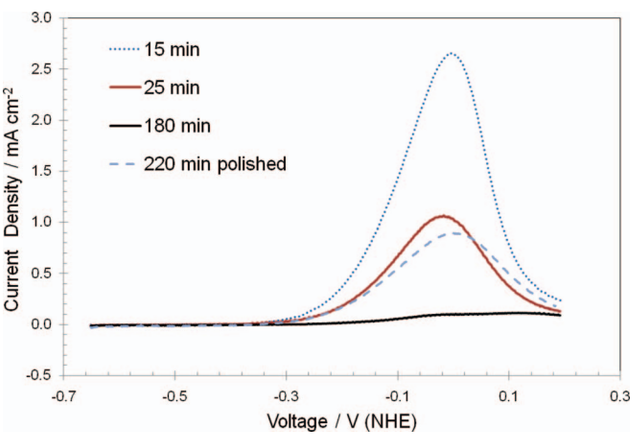

Figure 8. The effect of time on methanol oxidation in 1M MeOH and 0.1 M TMAOH at room temperature. Cyclic voltammetries were collected at 15, 25, and 180 minutes after the electrode was immersed in the solution. After 220 minutes, the electrode surface was polished on aluminum particles, and then the voltammogram was conducted in the same solution.

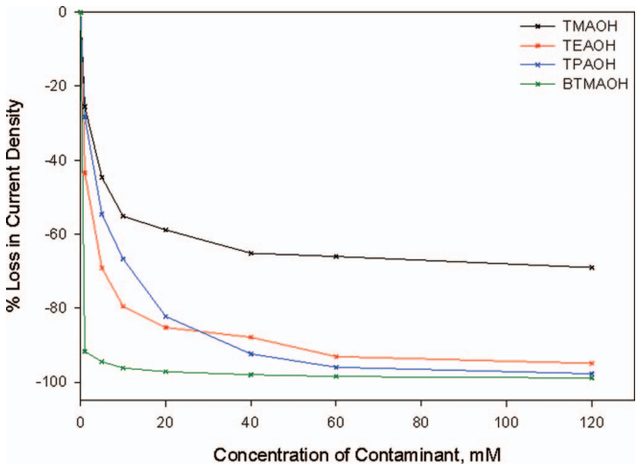

Figure 9. Percent loss in current density as a function of contaminant concentration in 0.1M KOH + 0.5M MeOH + x mM contaminant. Glassy carbon disk electrode (0.247 cm^2) with 5 μL of 30% Pt/C ink deposited (Loading = 7.5 ug_{Pt}/cm^2). Steady state currents obtained from chronoamperometry at 0.6V vs RHE at 900 seconds.

significant adsorption effect on the platinum surface resulting in loss of methanol oxidation activity. The decrease in current became more pronounced at higher concentrations of the added cations. TMA^+ showed the smallest drop in current, whereas the other three cations with bulkier substituent groups resulted in substantially greater loss in current. This observation is consistent with previous literature that showed a higher surface inhibition with the longer alkyl length on the ammonium group.[48]

These results with different quaternary ammonium cations in aqueous electrolytes show that quaternary ammonium ion adsorption on Pt surfaces lowers the rate of methanol oxidation by blockage of the active catalyst surface area. However, the solid polymer electrolyte, ion-conducting medium in a polymer-based fuel cell is different from that of free ions in an aqueous solution. A fuel cell electrode consists of quaternary ammonium cations with little chain segment mobility tethered to a polymer backbone. To better mimic the reaction medium in a fuel cell on a planar electrode surface, an anion exchange polymer with quaternary ammonium ion sites, PTMAOH was used as the electrolyte without additional alkali metal hydroxide. The polymer electrolyte provides high anion conductivity with high viscosity in the electrolyte phase, as would occur in a fuel cell electrode. The voltammogram for methanol oxidation in 0.1 M PTMAOH is shown in Figure 7 and a closer view shown in Figure 10. Unlike the voltammograms obtained in aqueous NaOH or TMAOH, the forward scan does not exhibit a clear oxidation peak for methanol in Figure 7, and the oxidation potential was shifted to more positive values, ca. 400mV, relative to the ones in TMAOH. The oxidation current increased slowly as the potential was scanned to 0.6 V. Interestingly the peak current on the backward scan is greater than the one on the forward scan. This behavior can arise from different effects including the following two contributing factors. When the electrode potential reached a very positive value, the quaternary ammonium cations could be repelled electrostatically from the electrode surface, making available catalytic sites for methanol oxidation on the reverse scan. Alternatively, surface poisoning intermediates formed at positive voltages by an interaction with ammonium groups can be removed.

The AEM fuel cell tests clearly show that the addition of free NaOH to a methanol solution improves the performance of AEM cells. Similarly, the onset potential of methanol oxidation shifted to more negative values and the magnitude of the oxidation current with 0.1 M NaOH in the solution was greater, as shown in Figure 10. This improvement was observed within 5 minutes after its addition of NaOH.

It is critical to note that the methanol oxidation in PTMAOH is substantially lower than in TMAOH. This cannot be due the fact that OH^- conductance in PTMAOH is lower than in KOH electrolyte. It is important to consider how the double layer structure is altered at the different electrolyte/Pt interfaces. The double layer is generally broken down into three distinct regions: the inner Helmholtz plane (IHP), the outer Helmholtz plane (OHP), and the diffuse layer. Figure 11 shows these three regions formed on a negatively charged electrode surface. Species located in the inner Helmholtz plane are said to be specifically adsorbed and define the IHP at a distance, x_1, determined by the electrical centers of the adsorbed species. The distance to which other, nonspecifically adsorbed species can approach the electrode surface is then limited by the thickness of compact layer. This is often considered the plane of closest approach and is defined as OHP at a distance, x_2. Nonspecifically adsorbed ions are distributed in a three dimensional region, called diffuse layer, from the OHP to the bulk of the solution. In solutions without specific adsorption, the Gouy-Chapman-Stern model describes the voltage drop in solution

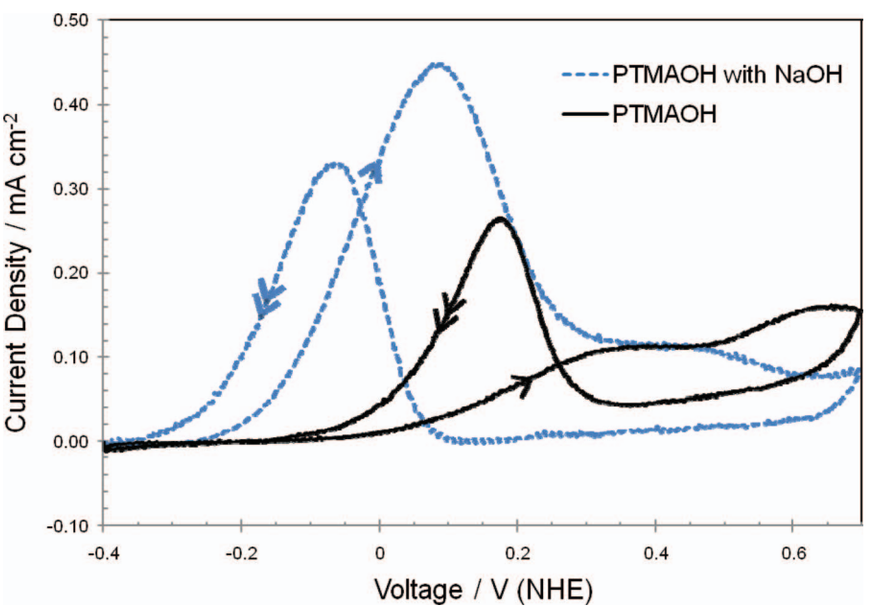

Figure 10. Cyclic voltammograms on Pt electrode in the solution of 1 M MeOH and 0.1 M PTMAOH with or without NaOH (0.1 M) addition. The scan rate is 10 mV s^{-1}. Single and double arrows are for forward and backward scans, respectively.

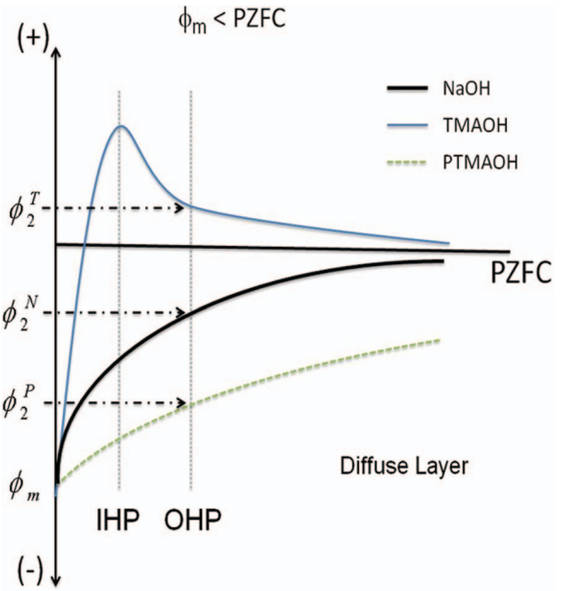

Figure 11. Expected potential profile of anode double layer interface in NaOH, TMAOH, and PTMAOH solutions when the electrode potential is more negative than PZC.

occurring across a compact and diffuse layer with the locus of centers of the hydrated ions of closest approach at the OHP.[49] In concentrated electrolytes, the potential difference across the double layer occurs primarily in the compact or inner layer with little contribution of the diffuse layer because there are abundant ions within close proximity of the surface to establish the compact layer. In dilute electrolytes, or ones where the ions have limited mobility, the potential drop across the diffuse layer becomes important and manifests itself in two ways, as described by the Frumkin effect. First, the electrode reaction is not driven by the potential difference, ϕ_m - ϕ_s, where ϕ_m is the metal potential and ϕ_s is the solution potential, but rather the electroactive species at the OHP experiences a potential difference of (ϕ_m - ϕ_2), where ϕ_2 is the potential at the OHP. In addition, charged electroactive species migrate under the influence of the electric field within the diffuse layer. The concentration of the electroactive species at the OHP will be different from that immediately outside the diffuse layer by a factor given by $\exp(-z\phi_2 F/RT)$, where z is the charge on the ion, F is Faraday's constant, R is the ideal gas constant, and T is the absolute temperature. In general, cations are attracted to the electrode surface when the surface has a negative charge ($E < E_{PZFC}$) while anions are repelled. Similarly, anions are attracted to a positive electrode surface ($E > E_{PZFC}$) while cations are repelled. As a result, at potentials positive of the PZFC an excess of anions will populate the IHP resulting in a negative shift of ϕ_2. Likewise, at negative potentials cations will be attracted to the surface resulting in a positive shift in ϕ_2. It is noteworthy to mention that $\phi_m = \phi_s = \phi_2$ at the PZFC.

These effects can have a profound influence on the kinetics of an electrode reaction since ϕ_2 varies with E - E_{PZC} and electrolyte concentration, this in turn are related to both the apparent rate constant and exchange current density, which are functions of ϕ_2.[50–52] This relationship is generally called Frumkin correction and allows relating the true rate constant, k_t^0, to the apparent one, k^0,by the following Equation.

$$k^0 = k_t^0 \exp\left[\frac{\alpha F \phi_2}{RT}\right] \exp\left[\frac{-zF\phi_2}{RT}\right] \quad [1]$$

The first exponential term is a correction factor for the potential driving the electrode reaction at OHP and valid for outer sphere electron transfer reactions. The second exponential term is the correction for concentration profile and applied for any charged species.

In the absence of specific adsorption, ϕ_2 can be predicted using the Gouy-Chapman-Stern model. However, in the case of specific adsorption of charged species, such as quaternary ammonium ions, the effects can become more complex. The specific adsorption of electro-inactive species can create significant changes in the structure of the double layer which differ from non-adsorbing case.[49,50,52] Specific adsorption of anions will make ϕ_2 more negative, while specific adsorption of cations will lead to more positive ϕ_2. In principle, these effects can be considered using Frumkin effect. However, the actual potential at the OHP cannot be defined; rather qualitative assessment can be made. It is also important to note that specific adsorption of ions also results in blockage of electrode surface, inhibiting the reaction rate, which is independent of ϕ_2. Typically, low concentrations of adsorbing species affect the reaction rate by ϕ_2 effect. When the concentration increases the surface blockage becomes dominant, suppressing ϕ_2 effect.

Methanol oxidation is an inner-sphere electron transfer reaction and methanol is a neutral molecule. Therefore, the Frumkin effect does not directly affect the methanol species. Instead, the oxidation of alcohols on platinum requires the presence of adsorbed hydroxide species to proceed through a Langmuir-Hinshelwood mechanism. Transport of hydroxide anions across the diffuse layer and subsequent specific adsorption on the electrode surface are necessary for alcohol oxidation. The concentration of hydroxide at the OHP, C_{OH}^{OHP}, available for adsorption is controlled by the bulk concentration, charge of the ion, and ϕ_2, as shown in below in Equation 2.

$$C_{OH}^{OHP} = C_{OH}^{bulk} \exp\left[\frac{-zF\phi_2}{RT}\right] \quad [2]$$

The double layer structure of an electrode-electrolyte interface significantly differs in polyelectrolyte and aqueous electrolytes. The double layer structures in NaOH, TMAOH, and polyelectrolyte surfaces are depicted for a negatively charged electrode surface in Figure 11. When the electrode potential is negative of PZC in a NaOH solution, there will be a potential gradient from the electrode to the bulk solution potential. In TMAOH solution, TMA^+ species are adsorbed on the Pt surface, particularly because $\phi_m < \phi_s$, forming a compact inner layer of positive charges. In contrast, TMA^+ moieties tethered to the PTMAOH polymer chain are not as mobile as free TMA^+ causing the excess charge in the electrolyte for $PTMA^+$ to be distributed across the a diffuse layer. The mobile TMA^+ cations can form a more compact double layer due to their mobility. These variations in the structure of the double layer result in large differences in ϕ_2. The order of ϕ_2 would be $\phi_2^T > \phi_2^N > \phi_2^P$ in TMAOH, NaOH, and PTMAOH, respectively. However, this order does not match the order of performances obtained for methanol oxidations in Figure 7. Even though, relatively more positive value of ϕ_2^T would favor the transport of hydroxide ions to the OHP, this factor is outweighed by the blockage of the electrode surface, decreasing the available catalyst surface area and oxidation rate.

When the TMAOH and PTMAOH solutions are considered, the TMA^+ cation is more mobile than the tethered $PTMA^+$ cation which could lead to a greater degree of adsorption and loss of catalyst surface area, however, $PTMA^+$ cations show smaller currents. The lower reaction rate in PTMAOH is probably due to the more negative value of ϕ_2^P than that of ϕ_2^T. The negative value of ϕ_2^P inhibits the transport of hydroxide to the electrode surface, limiting the reaction rate. This effect on hydroxide transport and adsorption explains the enhancement in the performance when alkali metal hydroxide is added to the fuel, shown in this study and the literature. The addition of NaOH to PTMAOH introduces two effects; (i) the bulk concentration of OH^- ions increases in 2 and (ii) the mobile Na ions lead to a decrease in the thickness of diffuse layer, resulting in lower ϕ_2. These changes lead to higher apparent reaction rates.

The proposed ϕ_2 effect on hydroxide transport and subsequent adsorption are difficult to quantify. Instead, charged redox couples were added to the electrolyte to help identify changes probe the double layer structure and consequent ϕ_2 effect. In this study, the

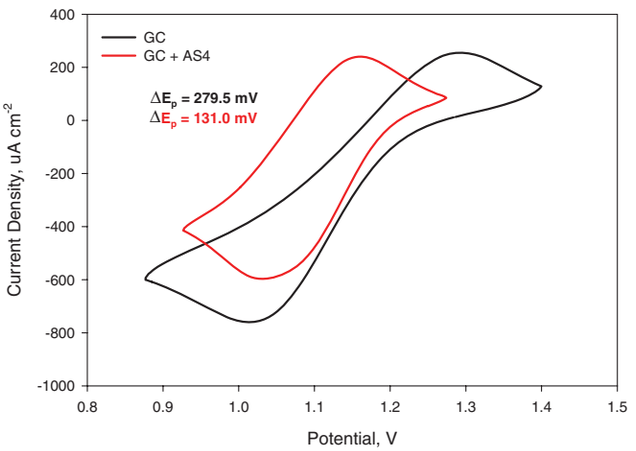

Figure 12. CV of $Fe(CN)_6^{3-/4-}$ redox couple in Ar saturated 0.1 M NaOH + 10 mM $K_3Fe(CN)_6$ solution. Scans performed on glassy carbon disk electrode with 5 μL of 5 wt.% AS4 ionomer deposited on surface. Geometric surface area = 0.247 cm^2. Scan rate = 20 mV/s.

$Fe(CN)_6^{3-/4-}$ and $Co(NH_3)_6^{2+/3+}$ redox couples were employed in order to probe the electrode surface for evidence of the ϕ_2 effect in anion exchange ionomers and membranes. Cyclic voltammetry was used to observe the redox behavior of each couple on a glassy carbon electrode in the presence and absence of an anion exchange ionomer film (Tokuyama, AS4 which contains quaternary ammonium cation ion-exchange groups). Figure 12 displays the cyclic voltammograms for the $Fe(CN)_6^{3-/4-}$ redox couple on a GC electrode with and without a deposited film of AS4 ionomer. Typically, the current magnitude cannot be used to make a direct comparison between solution and AEM environment because both concentration and diffusion coefficients changes. However, the difference between the oxidation and reduction peaks can be evaluated to define a change in reaction rates. From Fig. 12, it can be seen that the peak separation (ΔE_p) decreases from 279.5 mV in the absence of AS4 to 131.0 mV in presence of the AS4 ionomer film. In contrast, Figure 13 shows the CV profiles for the $Co(NH_3)_6^{2+/3+}$ redox couple on a GC electrode with and without a deposited film of AS4 ionomer. The current densities are lower with AS4 ionomer than without ionomer because AS4 ionomer mostly excludes positively charged species, decreasing the concentration on the electrode surface, i.e. lower current. However, it is critical to note that

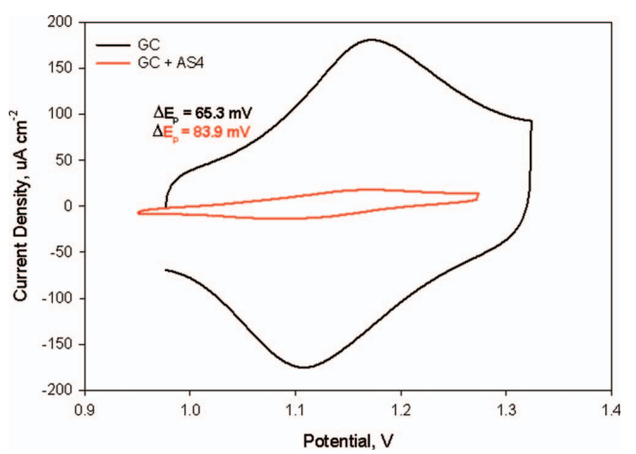

Figure 13. CV of $Co(NH_3)_6^{2+/3+}$ redox couple in Ar saturated 0.1 M NaOH + 10 mM $Co(NH_3)_6Cl_3$ solution. Scans performed on glassy carbon disk electrode with 5 μL of 5 wt.% AS4 ionomer deposited. Geometric surface area = 0.247 cm^2. Scan rate = 20 mV/s.

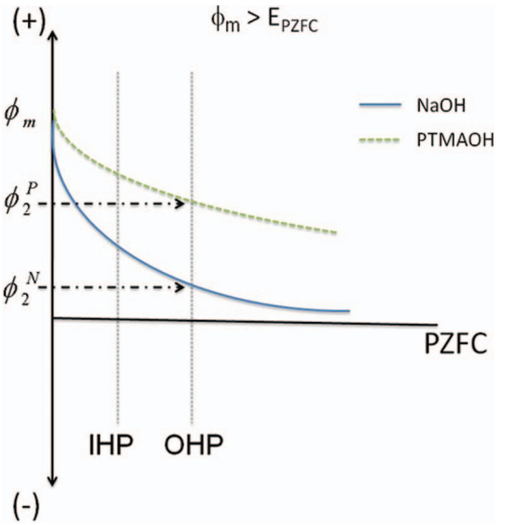

Figure 14. Expected potential profile of anode double layer interface in the presence and absence of anion exchange ionomer when the electrode potential is more positive than PZC.

there is a slight increase in ΔE_p from 65.3 mV to 83.9 mV in the presence of ionomer.

For these redox couples, the electrode potentials are more positive than PZC, ca. −0.1V, at the electron transfer potentials and the reaction occurs through an outer-sphere electron transfer pathway. The double layer structure differs from the methanol oxidation region where the electrode potential is more negative than PZC. Figure 14 shows the double layer structure when the electrode potential is greater than PZC in the presence and absence of AEM ionomer. As a distinct difference, the diffuse layer in an AEM becomes thicker relative to in the absence of an AEM. Consequently, ϕ_2 is more positive in the presence of AEM. For negatively charged redox couple, both exponential terms favor the electron transfer, i.e. higher kinetics. This is consistent with the lower peak splitting for $Fe(CN)_6^{3-/4-}$ in Figure 12. However, for positively charged species, the driving force still favors the reaction but the transport of these species is inhibited. This inhibition factor is greater than the enhancement in driving force, resulting in lower reaction kinetics. This is consistent with the greater peak splitting in Figure 13.

Summary

Quaternary ammonium cations in solution were shown to inhibit the oxidation of methanol through specific adsorption. The lower performance in polymer-bound ammonium cations relative to free ammonium cations, calls into question the structure of the double layer in AEM anodes. Specific adsorption, migration in the diffuse layer due to hydroxide repulsion away from the electrode, and possible ϕ_2 effects, all work against an efficient electrode structure until the anode potential becomes positive of PZFC. In this study, the effect of PZFC on anode operation was explored. Transition metal complexes in a polymer electrolyte showed behavior consistent with the ϕ_2 effect.

Acknowledgment

The authors gratefully acknowledge the intellectual contributions and financial support of the U.S. Army and DuPont Corporation, especially Deryn Chu (US Army) and Shoibal Banerjee (DuPont).

References

1. J. R. Varcoe and R. C. T. Slade, *Fuel Cells*, **5**, 187 (2005).
2. M. Ünlü, J. Zhou, and P. A. Kohl, *Electrochem. Solid-State Lett.*, **12**, B27 (2009).

3. M. Pourbaix, *Atlas of Electrochemical Equilibria in Aqueous Solutions* (Pergamon Press, Oxford, U.K., 1966), pp. 638.
4. J. S. Spendelow and A. Wieckowski, *Phys. Chem. Chem. Phys.*, **9**, 2654 (2007).
5. W. Sheng, H. A. Gasteiger, and Y. Shao-Horn, *J. Electrochem. Soc.*, **157**, B1529 (2010).
6. N. Ramaswamy and S. Mukerjee, *ECS Transactions*, **33**, 1777 (2010).
7. N. Ramaswamy, and S. Mukerjee, *J. Phys. Chem. C*, (2011) **115** (36), 18015–18026.
8. T. Zhang and A. B. Anderson, *J. Phys. Chem. C*, **111**, 8644 (2007).
9. N. Ramaswamy, R. J. Allen, and S. Mukerjee, *J. Phys. Chem. C*, (2011).
10. A. J. Appleby, *Comprehensive Treatise of Electrochemistry.* Vol. 7 Kinetics and Mechanisms of Electrode Processes (Plenum Press, New York, 1983) pp. 173.
11. A. V. Tripkovic et al., *Electrochim. Acta*, **47**, 3707 (2002).
12. J. L. Cohen, D. J. Volpe, and H. D. Abruna, *Phys. Chem. Chem. Phys.*, **9**, 49 (2007).
13. A. Schulze and E. Gulzow, *J. Power Sources*, **127**, 252 (Mar, 2004).
14. K. Matsuoka, Y. Iriyama, T. Abe, M. Matsuoka, and Z. Ogumi, *J. Power Sources*, **15**, 27 (2005).
15. J. R. Varcoe, R. C. T. Slade, G. L. Wright, and Y. Chen, *J. Phys. Chem. B*, **110**, 21041 (2006).
16. J. R. Varcoe and R. C. T. Slade, *Fuel Cells (Weinheim, Ger.)*, **5**, 187 (2005).
17. M. Ünlü, J. Zhou, and P. A. Kohl, *Fuel Cells*, **10**, 54 (2010).
18. H. A. Gasteiger, S. S. Kocha, B. Sompalli, and F. T. Wagner, *Appl. Catal., B*, **56**, 9 (2005).
19. M. Piana et al., *J. Power Sources*, **195**, 5875 (2010).
20. E. Antolini and E. R. Gonzalez, *J. Power Sources*, **195**, 3431 (2010).
21. H. Bunazawa and Y. Yamazaki, *J. Power Sources*, **182**, 48 (2008).
22. C. Coutanceau, L. Demarconnay, C. Lamy, and J. M. Leger, *J. Power Sources*, **156**, 14 (2006).
23. J. Kim, T. Momma, and T. Osaka, *J. Power Sources*, **189**, 999 (2009).
24. E. H. Yu and K. Scott, *J. Appl. Electrochem.*, **35**, 91 (2005).
25. J. R. Varcoe and R. C. T. Slade, *Electrochem. Commun.*, **8**, 839 (2006).
26. Y. S. Li, T. S. Zhao, J. B. Xu, S. Y. Shen, and W. W. Yang, *J. Power Sources*, **196**, 1802 (2011).
27. L. Demarconnay, S. Brimaud, C. Coutanceau, and J. M. Leger, *J. Electroanal. Chem.*, **601**, 169 (2007).
28. K. Matsuoka, Y. Iriyama, T. Abe, M. Matsuoka, and Z. Ogumi, *J. Power Sources*, **150**, 27 (2005).
29. Y. S. Li, T. S. Zhao, and Z. X. Liang, *J. Power Sources*, **190**, 223 (2009).
30. H. Kim et al., *Electrochim. Acta*, **56**, 3085 (2011).
31. B. Beden, F. Kadirgan, C. Lamy, and J. M. Leger, *J. Electroanal. Chem.*, **142**, 171 (1982).
32. J. Prabhuram and R. Manoharan, *J. Power Sources*, **74**, 54 (1998).
33. E. H. Yu, K. Scott, R. W. Reeve, L. Yang, and R. G. Allen, *Electrochim. Acta*, **49**, 2443 (2004).
34. Y. S. Li, T. S. Zhao, and Z. X. Liang, *J. Power Sources*, **187**, 387 (2009).
35. N. Fujiwara et al., *J. Power Sources*, **185**, 621 (2008).
36. H. Hou, G. S. R. He, Z. Wu, and B. Sun, *J. Power Sources*, **182**, 95 (2008).
37. C. Coutanceau, L. Demarconnay, C. Lamy, and J.-M. Leger, *J. Power Sources*, **156**, 14 (2006).
38. J. Kim, T. Momma, and T. Osaka, *J. Power Sources*, **189**, 999 (2009).
39. E. H. Yu and K. Scott, *J. Appl. Electrochem.*, **35**, 91 (2005).
40. E. H. Yu and K. Scott, *J. Power Sources*, **137**, 248 (2004).
41. S. Trasatti and O. A. Petrii, *Pure Appl. Chem.*, **63**, 711 (1991).
42. F. C. Anson, *Accounts Chem. Res.*, **8**, 400 (1975).
43. V. Climent, N. Garcia-Araez, E. Herrero, and J. Feliu, *Russ. J. Electrochem.*, **42**, 1145 (2006).
44. A. N. Frumkin and O. A. Petrii, *Electrochim. Acta*, **20**, 347 (1975).
45. J. O. Bockris, S. D. Argade, and E. Gileadi, *Electrochim. Acta*, **14**, 1259 (1969).
46. E. Gileadi, S. D. Argade, and J. O. Bockris, *J. Phys. Chem.*, **70**, 2044 (1966).
47. *Hydrogen Degradation of Ferrous Alloys* (Noyes Publications, New Jersey 1985) pp. 89.
48. L. Gierst, J. Tondeur, and E. Nicolas, *J. Electroanal. Chem.*, **10**, 397 (1965).
49. A. J. Bard and L. Faulkner, *Electrochemical Methods,* 2nd Edition, (Wiley, NY, 2001).
50. M. A. V. Devanathan and M. J. Fernando, *Trans. Faraday Soc.*, **58**, 368 (1962).
51. A. N. Frumkin, *Trans. Faraday Soc.*, **55**, 156 (1959).
52. M. Breiter, M. Kleinerman, and P. Delahay, *J. Am. Chem. Soc.*, **80**, 5111 (1958).